



Dynamic alteration in miRNA and mRNA expression profiles at different stages of chronic arsenic exposure-induced carcinogenesis in a human cell culture model of skin cancer

Mayukh Banerjee¹ · Ana Ferragut Cardoso¹ · Laila Al-Eryani^{1,7} · Jianmin Pan^{2,6} · Theodore S. Kalbfleisch^{3,8} · Sudhir Srivastava^{4,5} · Shesh N. Rai^{2,4,6} · J. Christopher States¹

Received: 7 April 2021 / Accepted: 17 May 2021 / Published online: 25 May 2021
© The Author(s) 2021

Abstract

Chronic arsenic exposure causes skin cancer, although the underlying molecular mechanisms are not well defined. Altered microRNA and mRNA expression likely play a pivotal role in carcinogenesis. Changes in genome-wide differential expression of miRNA and mRNA at 3 strategic time points upon chronic sodium arsenite (As^{3+}) exposure were investigated in a well-validated HaCaT cell line model of arsenic-induced cutaneous squamous cell carcinoma (cSCC). Quadruplicate independent HaCaT cell cultures were exposed to 0 or 100 nM As^{3+} for up to 28-weeks (wk). Cell growth was monitored throughout the course of exposure and epithelial-mesenchymal transition (EMT) was examined employing immunoblot. Differentially expressed miRNA and mRNA profiles were generated at 7, 19, and 28-wk by RNA-seq, followed by identification of differentially expressed mRNA targets of differentially expressed miRNAs through expression pairing at each time point. Pathway analyses were performed for total differentially expressed mRNAs and for the miRNA targeted mRNAs at each time point. RNA-seq predictions were validated by immunoblot of selected target proteins. While the As^{3+} -exposed cells grew slower initially, growth was equal to that of unexposed cells by 19-wk (transformation initiation), and exposed cells subsequently grew faster than passage-matched unexposed cells. As^{3+} -exposed cells had undergone EMT at 28-wk. Pathway analyses demonstrate dysregulation of carcinogenesis-related pathways and networks in a complex coordinated manner at each time point. Immunoblot data largely corroborate RNA-seq predictions in the endoplasmic reticulum stress (ER stress) pathway. This study provides a detailed molecular picture of changes occurring during the arsenic-induced transformation of human keratinocytes.

Keywords Arsenic · Skin carcinogenesis · Differential gene expression · Pathway analysis · Passage matching · Endoplasmic reticulum stress

✉ J. Christopher States
jcstates@louisville.edu

¹ Department of Pharmacology and Toxicology, University of Louisville, Louisville, KY, USA

² Biostatistics and Bioinformatics Facility, James Graham Brown Cancer Center, University of Louisville, Louisville, KY, USA

³ Department of Biochemistry and Molecular Genetics, University of Louisville, Louisville, KY, USA

⁴ Department of Bioinformatics and Biostatistics, University of Louisville, Louisville, KY, USA

⁵ Centre for Agricultural Bioinformatics, ICAR-Indian Agricultural Statistics Research Institute, New Delhi 110012, India

⁶ Biostatistics and Informatics Facility, Center for Integrative Environmental Health Sciences, University of Louisville, Louisville, KY, USA

⁷ Present Address: Knowledge Management and Special Projects Branch, Center for Strategic Scientific Initiatives (HNC1L), National Cancer Institute, National Institutes of Health, Bethesda, MD 20892, USA

⁸ Present Address: Gluck Equine Research Center, University of Kentucky, Lexington, KY, USA

Introduction

Chronic exposure to arsenic, a naturally occurring metalloid, adversely affects over 225 million people worldwide (Naujokas et al. 2013; Podgorski and Berg 2020). Arsenic is a Class I multi-organ carcinogen in humans (IARC. 2012), skin being the most common target organ (Karagas et al. 2015). Arsenic exposure is the second leading cause of skin cancer after UV in sunlight (Surdu 2014). Arsenic-induced cutaneous squamous cell carcinoma (cSCC) is common in exposed human populations (Banerjee 2011) and is extremely invasive with a high rate of recurrence and fatality (Waldman and Schmults 2019). Although studied extensively, molecular mechanisms of arsenic-induced skin carcinogenesis are still controversial [reviewed in (Hunt et al. 2014)].

Lack of animal model systems has hindered understanding the events leading up to chronic arsenic exposure induced skin cancers. It has never been possible to induce skin cancer in rodents with arsenic exposure alone, even at exposures of 50 ppm (Tokar 2016), which far exceeds the environmental exposure levels human populations encounter (Ghosh et al. 2007; Gonsebatt et al. 1994; Nigra et al. 2020).

Epidemiological studies demonstrate that mean blood arsenic levels of human populations chronically exposed to 100–300 ppb arsenic in drinking water is about 100 nM (Gonsebatt et al. 1994, 1997; Pi et al. 2000). Primary human skin keratinocyte lines transformed through chronic exposure to *in vivo* levels induced by environmentally relevant levels of arsenite (As^{3+}) would be ideal to study the molecular mechanisms involved in arsenic-induced cSCC. Unfortunately, primary cell lines undergo only 16–20 passages before they become senescent, too short for chronic exposure regimes. The other option is to study skin tissues from exposed human populations. A handful of studies, including from our group, have employed this approach to dissect the underlying mechanisms of arsenic-induced skin cancers (Al-Eryani et al. 2018a; Guo et al. 2016). However, one inherent issue with such studies is, they look at the endpoint after the transformation has occurred, leaving a substantial knowledge gap in understanding the molecular events leading up to a transformed phenotype. In absence of this knowledge, it is difficult to understand if the changes observed are causes or effects of transformation.

Most of the current knowledge about arsenic carcinogenesis is gained from studies on cell line models treated with arsenic. Unfortunately, many of the studies have used high arsenic concentrations (micromolar to millimolar) and short exposure duration (hours to days). Arsenic is well known to have hormetic effects upon a variety of

molecules and cellular pathways (Calabrese and Baldwin 2003; Hashmi et al. 2014) making it difficult to extrapolate the results meaningfully to chronically exposed populations. Moreover, most of these studies look at one or few endpoints at the end of the exposure regime. Thus, they offer only a limited view of the molecules and pathways that represent a small fraction of complex interactions and dysregulation of multiple networks occurring simultaneously upon As^{3+} exposure.

Fortunately, immortalized human keratinocytes (HaCaT) are an *in vitro* model for normal human keratinocytes (Boukamp et al. 1988) that can be used to study arsenic-induced skin cancer (Pi et al. 2008). Pi et al. showed that continuous exposure of HaCaT cells for 28-wk to a low level (100 nM) of sodium arsenite transformed these cells and resulted in an aggressive squamous cell carcinoma phenotype upon inoculation of nude mice (Pi et al. 2008). Previous studies in our laboratory showed that chronic As^{3+} exposure for 7-wk led to differential small RNA and mRNA expression (Al-Eryani et al. 2017). HaCaT cells chronically exposed to 100 nM NaAsO_2 were observed to grow slower until 19–20-wk when transformation starts (Pi et al. 2008; Sun et al. 2009). A third important time point to study in the transformation path is 28-wk by which time cells are transformed (Pi et al. 2008). Importantly, the As^{3+} exposure used reflects the actual mean blood arsenic levels of chronically exposed populations (Gonsebatt et al. 1994, 1997; Pi et al. 2000), and is thus toxicologically and environmentally relevant. This well-established model thus provides an excellent opportunity to explore the molecular events happening as a function of time starting from the initiation of exposure through to the cells acquiring cSCC phenotype. The current study aimed to provide an understanding of the complex interactions of miRNA, mRNA and the pathways and networks they regulate at these three critical times during chronic As^{3+} exposure-induced cSCC.

Thus, a longitudinal study was performed to determine miRNA and mRNA differential expression in HaCaT cells chronically exposed to 100 nM NaAsO_2 at 3 time points: 7-wk (early transformation related changes), 19-wk (start of actual transformation) and 28-wk (fully transformed cells). Employing a state-of-the-art RNA-seq platform, we show that at each time point, a considerable number of miRNAs and mRNAs are being differentially regulated in As^{3+} -exposed HaCaT cells compared to passage-matched unexposed cells. Through expression pairing analysis, we show that the differentially expressed mRNAs at each time point are targeted by the differentially expressed miRNAs at that time point. Furthermore, we demonstrate that at each time point pathways known to be involved in carcinogenesis are being dysregulated and that these dysregulated pathways interact extensively as complex networks. Furthermore, we validate the RNA-seq predictions at the protein level through

immunoblot for several molecules involved in the endoplasmic reticulum (ER) stress pathway. Our study reflects the dynamic and temporally labile mechanisms by which major biochemical pathways are regulated by chronic As³⁺ exposure ultimately leading to cSCC.

Materials and methods

Chemicals

Sodium arsenite (NaAsO₂; CAS 7784–0698) was obtained from Thermo Fisher Scientific Inc. (Waltham, MA, USA). Single-thaw aliquots of sodium arsenite were prepared in UltraPure™ DNase/RNase-Free Distilled Water (Thermo Fisher Scientific Inc.) and were thawed immediately before use. MEM alpha modification media, trypsin, ethylene diamine tetraacetic acid and penicillin/ streptomycin were obtained from Thermo Fisher Scientific Inc. Fetal Bovine Serum (characterized) was obtained from Hyclone (Logan, UT, USA). All other chemicals were obtained from Thermo Fisher Scientific Inc., unless specifically mentioned.

Cell Culture

The HaCaT model of Pi et al. (2008) was adopted for the present study. HaCaT cells were the kind gift of Dr. TaiHao Quan, University of Michigan. HaCaT cell cultures were maintained as independent quadruplicates (4 with and 4 without 100 nM NaAsO₂) for 28-wk. The cells were cultured in MEM alpha modification media supplemented with 10% fetal bovine serum, 100 units/mL penicillin/100 µg/mL streptomycin and 2 mM glutamine. Cultures were maintained at 37 °C in a humidified 5% CO₂ atmosphere. Cells were passaged twice a week and 10⁶ cells were plated per 100 mm dish every time. At each passage, the total cells were counted for calculation of population doubling. Identity of cultures as HaCaT cells was confirmed by STR mapping (Genetica, Burlington, NC).

Total RNA isolation

In order to isolate total RNA (including mRNA and small RNA) from cells harvested at 7, 19 and 28-wk time points, mirVana™ RNA isolation kit was employed as described previously (Al-Eryani et al. 2018b) following the manufacturer's recommendations. The quality of the isolated RNA was determined using the Agilent RNA 6000 Pico Kit, Eukaryote, version 2.6 and the Agilent 2100 Bioanalyzer instrument (Agilent Technologies, Inc., Santa Clara, CA, USA). All samples used had RIN (RNA integrity number) > 9.

miRNA library preparation, cluster generation and sequencing

Library preparation, cluster generation and sequencing of all 24 samples were performed in the Center for Genetics and Molecular Medicine (CGeMM) DNA Facility Core at the University of Louisville. The Truseq Small RNA kit was used to prepare miRNA libraries from 1 µg total RNA. Each Library was individually gel purified on a Novex TBE 6% gel and resuspended in 10 µL 10 mM Tris–HCl, pH 8.5. Libraries were subsequently validated and quantitated by running 1 µL sample on the Agilent Technologies 2100 Bioanalyzer DNA High Sensitivity Chip. Thirty-six-cycle single sequencing reads were generated on the Illumina NextSeq500 instrument utilizing the 500 High output v2 (75 cycle) sequencing kit.

mRNA library preparation, cluster generation and sequencing

The Truseq Stranded mRNA kit was used to prepare mRNA libraries from 1 µg total RNA. Libraries were validated on the Agilent 2100 Bioanalyzer and quantitated using the Illumina Library Quantification Kit, ABI Prism qPCR Mix from Kapa Biosystems and the ABI7900HT real-time PCR instrument. All samples were pooled and run simultaneously on 4 flow cells, using 2 × 150 paired end sequencing with the 500 High-output v2 (300 cycles) sequencing kit on the Illumina NextSeq500 instrument.

Data mapping

Paired end RNA-Seq data were generated for each experimental condition. The data for each replicate were stored, trimmed, mapped, and quantified individually. For miRNA, the newly generated reads were trimmed using Trimalore (Martin 2011) followed by pre-processing and subsequent analysis using miRDeep2 v:0.0.8 (Friedlander et al. 2012). The trimmed reads were mapped to the human reference genome hg19 (NCBI build 37.1 released 2009) using the RNA-Seq mapping software TopHat (Trapnell et al. 2012) and annotated transcripts were quantified in units of Fragments Per Kilobase of transcript per Million mapped reads (FPKM) using Cufflinks (Trapnell et al. 2012). The gene annotation used for the quantification was downloaded from ENSEMBL (version 81). All the ribosomal RNA (rRNA) and mitochondrial tRNA were removed to ensure that they would not influence the derived FPKM values. Further details on the pipeline and algorithms used for data mapping and analysis are provided in the Supplementary Methods. Data have been deposited in the GEO database, accession number GSE153057. For analysis of differential expression of mRNA, the RNA seq data was first checked for quality

control using FastQC v0.11.8 (Wingett and Andrews 2018). Data trimming was done using Trimmomatic version 0.38 (Bolger et al. 2014). Sequence alignment was performed by Star 2.6 (Dobin et al. 2013; Dobin and Gingeras 2015) against human genome reference from Ensembl (Release 95) (Schneider et al. 2017; Zerbino et al. 2018). Feature count was done using the R package “Rsubread” (Liao et al. 2013). Data have been deposited in the GEO database, accession number GSE107054.

RNA-Seq data analysis

For miRNA, data analysis was performed by comparing the log values of the counts generated from the sample reads + 0.00001 of exposed cells to the passage matched unexposed cells at each time point tested. The fold changes of the compared values were calculated using the equation: $FC = \text{mean}(\text{Exposed counts} + 0.00001) / \text{mean}(\text{Unexposed counts} + 0.00001)$. The *p*-values for these comparisons were calculated by two sample t-Test with equal variances (*p*_Eq). Differentially expressed miRNA at each time point was defined as *p*_Eq < 0.05. All analyses were obtained using SAS System V9. Cary, NC: SAS Institute Inc, 2003. For differential expression of mRNA, first genes having 0 values in all the samples for a single time point were removed from the dataset. The remaining data were analyzed for differential gene expression employing the R package “edgeR” (McCarthy et al. 2012; Robinson et al. 2010). Trimmed mean of M values (TMM) was used for normalization of the data for all the comparisons (Robinson and Oshlack 2010), while exact test (exactTest function) was employed for testing the significance of the difference in gene expression (Robinson and Smyth 2008). Differentially expressed mRNA molecules were defined as *p* < 0.01 and FC > ± 30% compared to passage-matched unexposed HaCaT cells.

Pathway analyses

Differentially expressed miRNA (*p*_Eq < 0.05) and mRNA molecules (*p* < 0.01 and FC > ± 30%) were analyzed by Ingenuity® Pathway Analysis (IPA®) (Qiagen Inc.). IPA® core analysis was performed on the differentially expressed mRNA dataset to generate a prediction of dysregulated canonical pathways at each time point. Pathways with $-\log(\text{p-value}) > 1.3$ and $IZ\text{-scoreI} > \pm 1$ was used to predict activation/inhibition status of the pathways. Z-score > 1 was activated, while Z-score < -1 was inhibited. Furthermore, differentially expressed mature miRNA molecules at each time point (as identified by IPA®) were expression paired with differentially expressed mRNA molecules at each time point to identify differentially expressed mRNA targets of differentially expressed miRNA molecules at each time point. IPA® core analysis was subsequently performed on

the differentially expressed mRNA targets of differentially expressed miRNAs dataset to generate a prediction of dysregulated canonical pathways at each time point. Figures for pathway interactions based on our differentially expressed mRNA data were prepared using IPA®.

Immunoblotting

Immunoblotting was performed to examine EMT and the protein expression status of selected ER stress pathway molecules at all three-time points. Sample preparation, estimation of protein content, and immunoblotting, and image acquisition was performed as described previously (Banerjee et al. 2020). Details regarding the antibodies used and their dilutions are presented in Supplementary Table 1. Raw data for densitometric analysis was generated from the images employing Image J software (Schneider et al. 2012).

Statistical analysis

Cell population doublings were calculated from total cell numbers for each independent culture at each passage. Mean cumulative doubling number (along with SD as a measure of error) for passage matched unexposed and As³⁺ exposed samples were plotted against time to generate the growth curve. The data were analyzed using R (R-Core-Team 2018) by two-way ANOVA followed by Tukey’s post-hoc test; *p*-value ≤ 0.05 was considered significant (Tukey 1949). Densitometric data for EMT and ER stress markers were analyzed using an unpaired two-tailed *t*-test; *p*-value ≤ 0.05 was considered significant. For each molecule at each time point, the mean of the unexposed samples was set to 100% and data were expressed as % mean unexposed at that time point. Densitometric analysis, heat maps, and bar graphs were generated using GraphPad Prism 9.0.1 (GraphPad Software, San Diego, CA, USA). Venn diagrams were generated employing the Venn Diagram Plotter program (<https://omics.pnl.gov/software/venn-diagram-plotter>).

Results

As³⁺ exposure alters the growth curve pattern and induces EMT

The growth curve data are represented in Fig. 1A. Comparison of mean cumulative cell doubling in As³⁺-exposed HaCaT cells to corresponding passage matched unexposed controls revealed that growth rates of As³⁺ exposed cells were slower at several times points prior to 19-wk. At 19-wk, the growth rates of As³⁺ exposed cells became similar to passage matched unexposed cells, while at later time points, As³⁺-exposed cells grew significantly faster. In conjunction

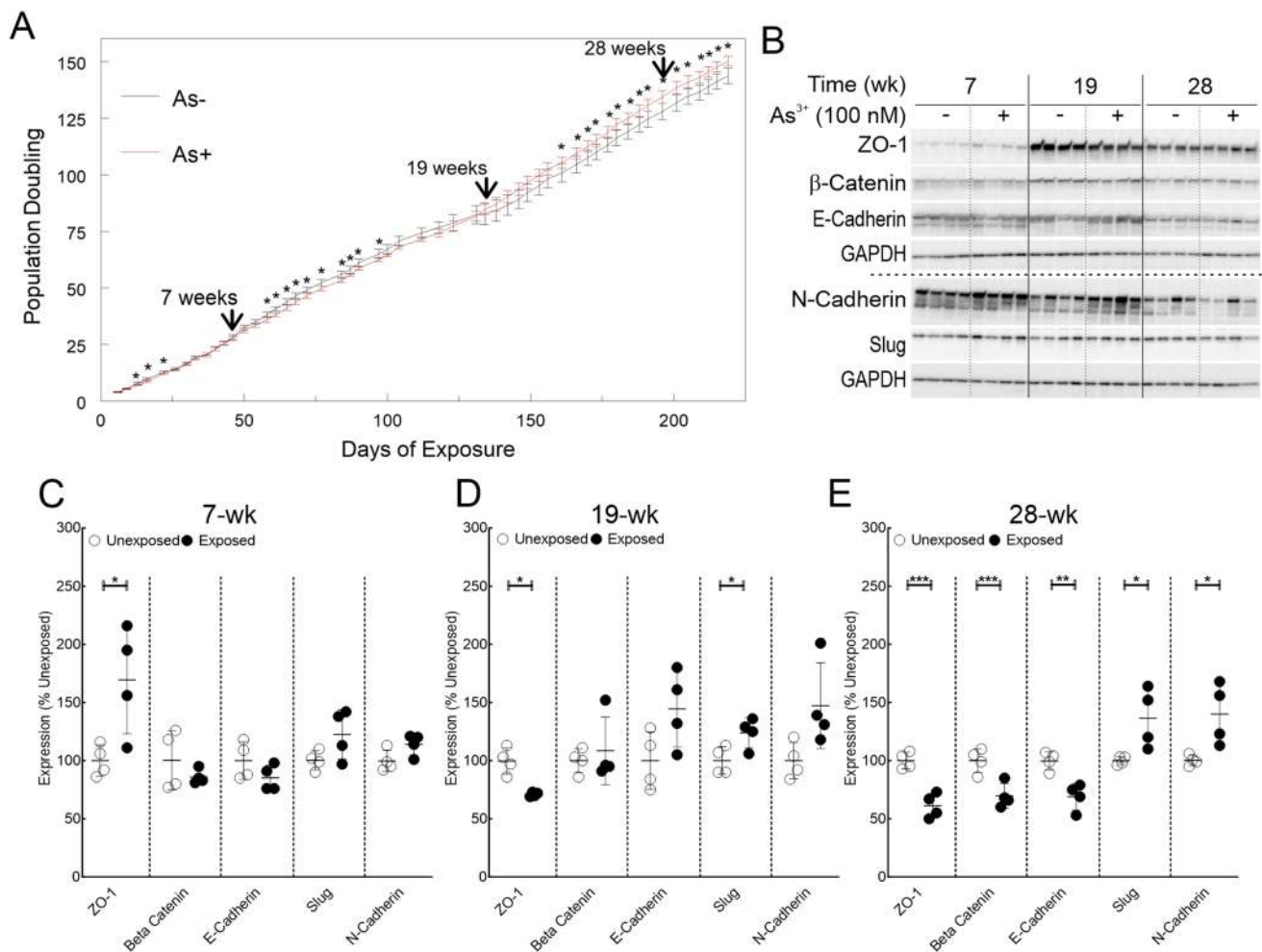


Fig. 1 Chronic As^{3+} exposure leads to altered growth rate and EMT. **A** Impact of As^{3+} exposure on cumulative HaCaT cell population doubling. Quadruplicate independent HaCaT cell cultures were incubated with 0 or 100 nM As^{3+} . Population doublings were calculated and the means \pm SD of cumulative doubling at each passage were plotted. Statistical analysis was done by two-way ANOVA, $*p \leq 0.05$. **B** Immunoblot for EMT markers at 7, 19 and 28-wk time points in

HaCaT cells exposed to 100 nM As^{3+} or passage matched unexposed controls. **C** Densitometric analysis of EMT marker expression at 7-wk. **D** Densitometric analysis of EMT marker expression at 19-wk. **E** Densitometric analysis of EMT marker expression at 28-wk. Protein expression data in panels **C–E** are plotted as means \pm SD and expressed as % mean unexposed. Statistical analysis was done by unpaired two-tailed *t*-test; $*p \leq 0.05$, $**p \leq 0.01$; $***p \leq 0.001$

with changes in the growth pattern, As^{3+} -exposed cells had undergone EMT upon 28-wk of exposure (Fig. 1B–E) as demonstrated by suppression of epithelial markers (ZO-1, β -Catenin and E-Cadherin) and concomitant induction of mesenchymal markers (Slug and N-Cadherin). Interestingly, even at 19-wk of exposure, ZO-1 was suppressed, and Slug induced (Fig. 1B, D). These data together with alteration in cell growth rate strengthen the notion that As^{3+} -exposed cells begin transforming around 19-wk.

As^{3+} exposure induces differential miRNA and mRNA expression pattern with time

More than 50 miRNAs were differentially expressed between As^{3+} -exposed and unexposed HaCaT cells at each

time point, with the most (124) at 19-wk (Fig. 2A–C). Data on individual differentially expressed miRNAs at each time point are presented in Supplementary Table 2. Longitudinal comparison showed that most of the differentially expressed miRNAs were unique to one-time point (Fig. 2B–C) only, with relatively few miRNAs being differentially expressed at two-time points (irrespective of induction or suppression status). Only one miRNA (hsa-miR-6733) was represented at all three-time points and was consistently suppressed (Fig. 2B–C; Supplementary Table 2). These data indicate that the miRNA landscape is markedly different at each phase of transformation.

Examination of the mRNA data revealed that 2706, 972 and 539 molecules were differentially expressed in As^{3+} exposed cells compared to passage matched unexposed cells

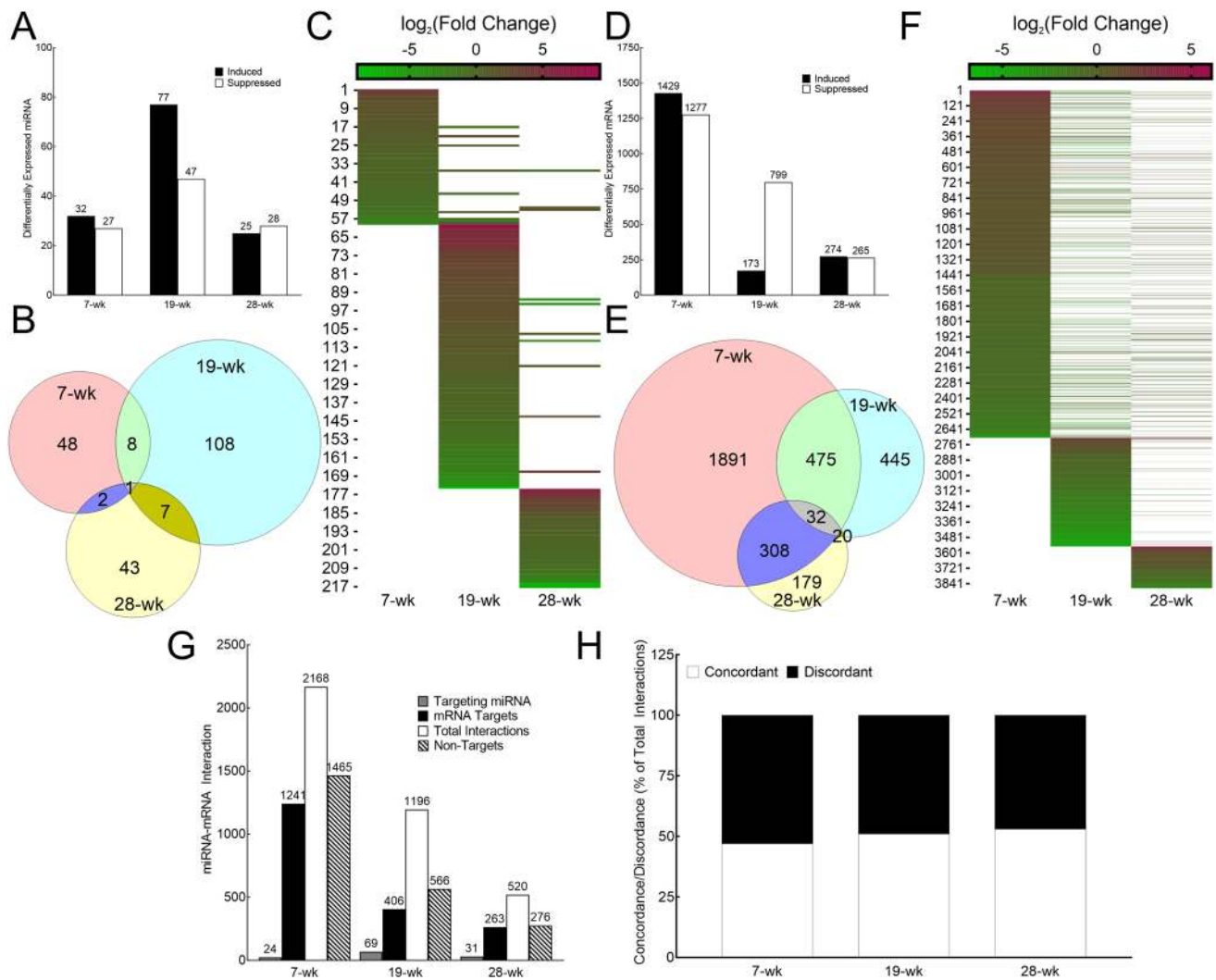


Fig. 2 Chronic As³⁺ exposure changes the landscape of differentially expressed miRNAs and mRNAs in a longitudinal manner. **A** Bar graph showing the number of miRNA molecules at 7, 19 and 28-wk time points differentially expressed in HaCaT cells exposed to 100 nM As³⁺ compared with passage matched unexposed controls (induced: closed bars; suppressed: open bars). Differential expression is defined as p_{Eq} < 0.05. **B** Venn diagram depicting the distribution of differentially expressed miRNAs (p_{Eq} < 0.05) at each time point along with the number of overlaps at different time points. **C** Heat Map of differentially expressed miRNA molecules at 7, 19 and 28-wk. The numerals on the y axis refers to the serial numbers assigned to the differentially expressed miRNA molecules in Supplementary Table 2. The color code bar on top refers to the log₂(Fold Change) expression values. Absence of a bar (represented by white) signifies either that miRNA molecule was not detected at that time point or was not differentially expressed at that time point. **D** Bar graph showing the number of mRNA molecules at 7, 19 and 28-wk time points differentially expressed in HaCaT cells exposed to 100 nM As³⁺ compared with passage matched unexposed controls (induced: closed bars; suppressed: open bars). Differential expression is defined as p < 0.01 and FC ± > 30%. **E** Venn diagram depicting the distribution of differentially expressed mRNAs (p < 0.01 and

FC ± > 30%) at each time point along with the number of overlaps at different time points. **F** Heat Map of differentially expressed mRNA molecules at 7, 19 and 28-wk. The numerals on the y axis refers to the serial numbers assigned to the differentially expressed miRNA molecules in Supplementary Table 3. The color code bar on top refers to the log₂(Fold Change) expression values. Absence of a bar (represented by white) signifies either that mRNA molecule was not detected at that time point or was not differentially expressed at that time point. **G** Expression pairing between differentially expressed miRNA and differentially expressed mRNA at 7, 19 and 28-wk. For each time point, shown are the total number of differentially expressed miRNA molecules that are targeting one or more differentially expressed mRNA molecules (light grey bars); the number of differentially mRNA molecules that are targeted by one or more differentially expressed miRNA molecules (closed bars), total number of miRNA-mRNA pairings (open bars) and the number of differentially expressed mRNA molecules that are not predicted to be targeted by any differentially expressed miRNA molecule (hatched bars). **H** Concordance–discordance relationship between differentially expressed miRNA and differentially expressed mRNA at 7, 19 and 28-wk. The data is presented as % of total interactions predicted at that time point

at 7, 19 and 28-wk time points respectively (Fig. 2D–F). Data on individual differentially expressed mRNAs at each time point is presented in Supplementary Table 3. The longitudinal comparison showed that most of the differentially expressed miRNAs were unique to 7 and 19-wk time points, while those differentially expressed at 28-wk time point had considerable overlap with those at 7-wk time point but not with 19-wk time point (Fig. 2E–F). As seen for miRNAs, the mRNA data indicate that the mRNA landscape is markedly different at each phase of transformation.

We were further interested in examining if the differentially expressed miRNA molecules could explain the differentially expressed mRNA molecules at each time point. Expression pairing analysis demonstrated that 42–49% of the differentially expressed mRNA molecules are being targeted by the differentially expressed miRNAs depending on the time point (Fig. 2G). Several differentially expressed mRNA molecules at each time point can be targeted by more than one differentially expressed miRNA, resulting in 2168, 1196, and 520 miRNA–mRNA pairings at 7, 19, and 28-wk time points respectively (Fig. 2G). Individual miRNA–mRNA pairing data at each time point is provided in Supplementary Table 4. As shown in Fig. 2H, at each time point ~50% of the pairings were found to be concordant (inverse expression relationship between differentially expressed miRNA and its differentially expressed target mRNA). It was also found that several differentially expressed mRNA molecules at each time point were being targeted by several differentially expressed miRNA molecules (Supplementary Table 4), which, in part could explain some of the discordance in the dataset.

As³⁺ exposure dysregulates multiple canonical pathways in a temporally dynamic manner

IPA® analysis of differentially expressed mRNAs revealed numerous biochemical pathways to be activated/inhibited upon chronic As³⁺ exposure at each time point (Fig. 3A). The activation/inhibition status of the predicted dysregulated pathways based on the differentially expressed mRNA molecules at each time point are depicted in Fig. 3B and Supplementary Table 5. The longitudinal comparison demonstrates that most of the predicted dysregulated pathways at 7 and 19-wk time points are not dysregulated at other time points. However, 2 of the 6 predicted dysregulated pathways at 28-wk are also dysregulated at 7-wk, while 1 more (osteoarthritis pathway) is dysregulated at all three timepoints (Fig. 3B–C) and is activated at 7 wk but inhibited at the two later time points. These data are consistent with the mRNA data indicating that the gene expression landscape is markedly different at each time during transformation.

Next, we wanted to explore if differentially expressed mRNA targets of differentially expressed miRNA molecules

would be consistent with these dysregulated pathways predictions of total differentially expressed mRNAs. Therefore, we performed a nested pathway analysis based only on the differentially expressed mRNA that were targeted by differentially expressed miRNA at each time point (Supplementary Fig. 1A–B). Pathways predicted to be activated/inhibited based on the subset of differentially expressed mRNA targeted by differentially expressed miRNA (Supplementary Table 6) demonstrated 65–81% overlap with the pathways predicted based on entire differentially expressed mRNA data depending on the time point (Fig. 3D). More detailed comparison of the pathways predicted based on the two analyses is presented in Supplementary Fig. 1C.

Corroboration of RNA-Seq and pathway analysis prediction of ER stress pathway inhibition at the protein level

ER stress pathway and its interaction with unfolded protein response are well characterized to play pivotal role in carcinogenesis (Chen and Cubillos-Ruiz 2020). Therefore, the ER stress pathway was selected to validate the RNA-seq data and pathway analysis predictions at the protein level. This pathway is predicted to be inhibited at both 7 and 28-wk, but not at 19-wk in both the total mRNA dataset analysis as well as the subset analysis (Fig. 3B, C; Supplementary Tables 5 and 6). Furthermore, while the pathway was predicted to be inhibited at two-time points, several molecules were differently modulated between the two-time points (Supplementary Fig. 2). This provided an ideal opportunity to examine if the RNA-seq data and the IPA pathway predictions can be validated at the level of protein expression. To assess if the RNA-seq predictions hold true at the protein level, we selected 8 molecules in the ER stress pathway as shown in Supplementary Fig. 2 (ATF4, BCL2, BIP, CHOP, IRE1, HSP72, NRF2 and PERK).

Immunoblot data for ER stress markers at three time points presented in Fig. 4A. Several of the proteins analyzed show time-dependent expression patterns in addition to As³⁺-dependent expression highlighting the importance of passage-matched controls. Densitometric analysis (Fig. 4B–D) corroborates the RNA seq predictions for 4 out of 8 molecules at all three-time points (ATF4, HSP72, NRF2 and PERK), 2 molecules at two-time points (BCL2 at 7 & 28-wk and CHOP at 7 & 19-wk) and remaining 2 molecules for one-time point each (BIP at 28-wk and IRE1 at 19-wk). These results support the predictions made by analyses of the RNA data.

Discussion

Mechanisms of chronic arsenic-exposure-induced carcinogenesis are widely studied, but a clear picture is far from emerging. A multitude of mechanisms has been implicated

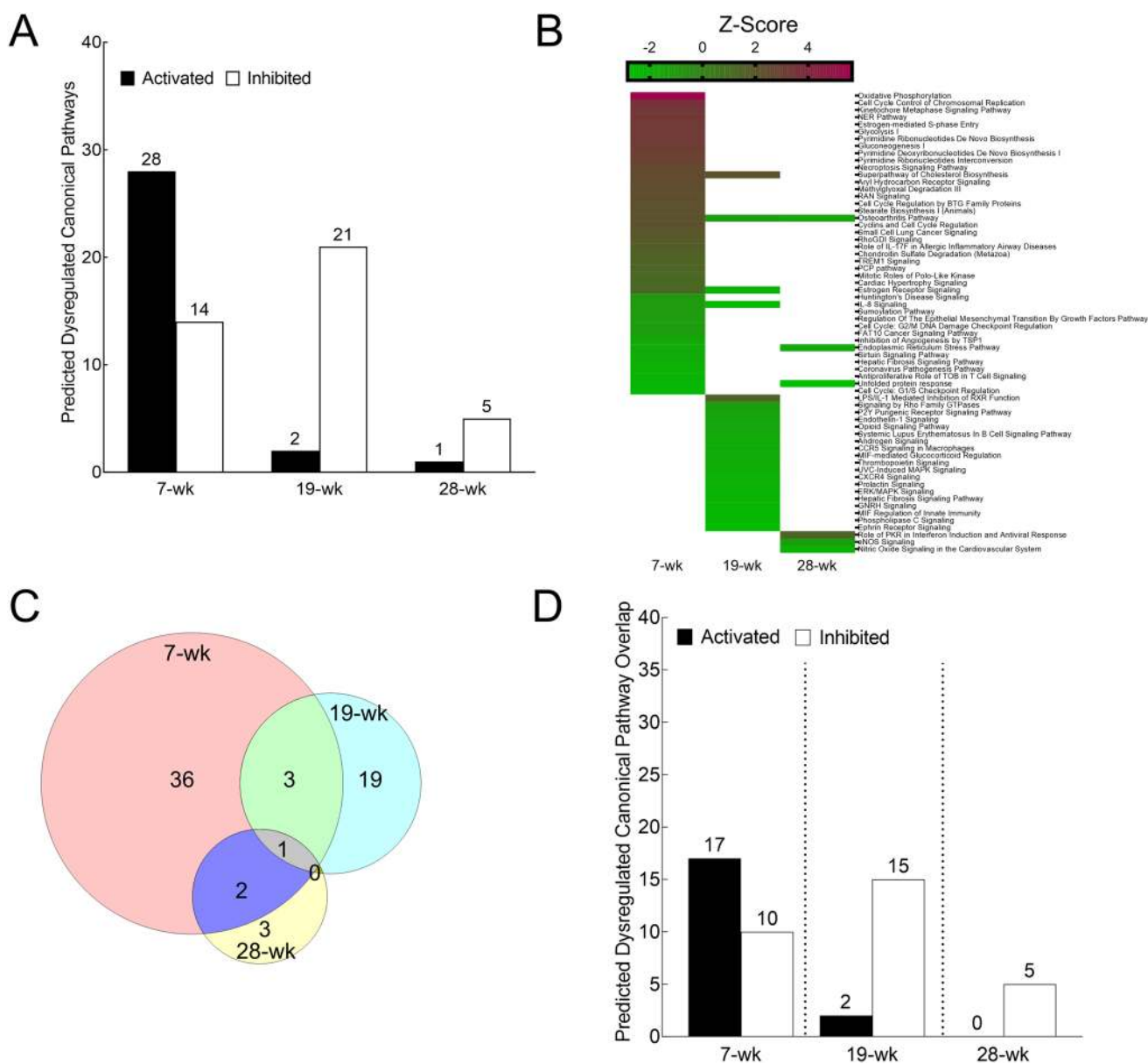


Fig. 3 Chronic As^{3+} exposure leads to widespread dysregulation in predicted canonical pathways in a longitudinal manner. **A** Bar graph showing the number of predicted dysregulated pathways at 7, 19 and 28-wk time points in HaCaT cells exposed to 100 nM As^{3+} compared with passage matched unexposed controls (activated: closed bars; inhibited: open bars). Activation is defined as $-\log(p\text{-value}) > 1.3$; $Z\text{-score} > 1$, while inhibition is defined as $-\log(p\text{-value}) > 1.3$; $Z\text{-score} < -1$. **B** Heat Map of predicted activated/inhibited pathways based on all differentially expressed mRNA molecules at 7, 19 and 28-wk (presented in the same order as in Supplementary Table 5). The color code bar on top refers to the Z-score values. Absence of

a bar (represented by white) signifies that the pathway was not predicted to be activated or inhibited at that time point. **C** Venn diagram depicting the distribution of predicted dysregulated pathways [$-\log(p\text{-value}) > 1.3$; $Z\text{-score} > \pm 1$] at each time point along with the number of overlaps at different time points. **D** Bar graph showing the number of pathways at 7, 19 and 28-wk time points predicted to be activated/inhibited both by the differentially expressed mRNA dataset (presented in Supplementary Table 5) as well as the differentially expressed mRNA targets of differentially expressed miRNA dataset (Presented in Supplementary Table 6)

and debated for their putative role in arsenic-induced carcinogenesis (Chen and Costa 2018; Cohen et al. 2016; Huang et al. 2019; Lee and Yu 2016; States 2015; Zhou and Xi 2018). It is well established that transcriptomic and proteomic profiles are globally altered in arsenic-induced

cancer tissues or in arsenic-transformed cell lines (Guo et al. 2016; Mir et al. 2017). Furthermore, experimental data from our group and others indicate that such genome-wide differential expression might be regulated partly by differential expression of miRNAs (Al-Eryani 2017; Al-Eryani

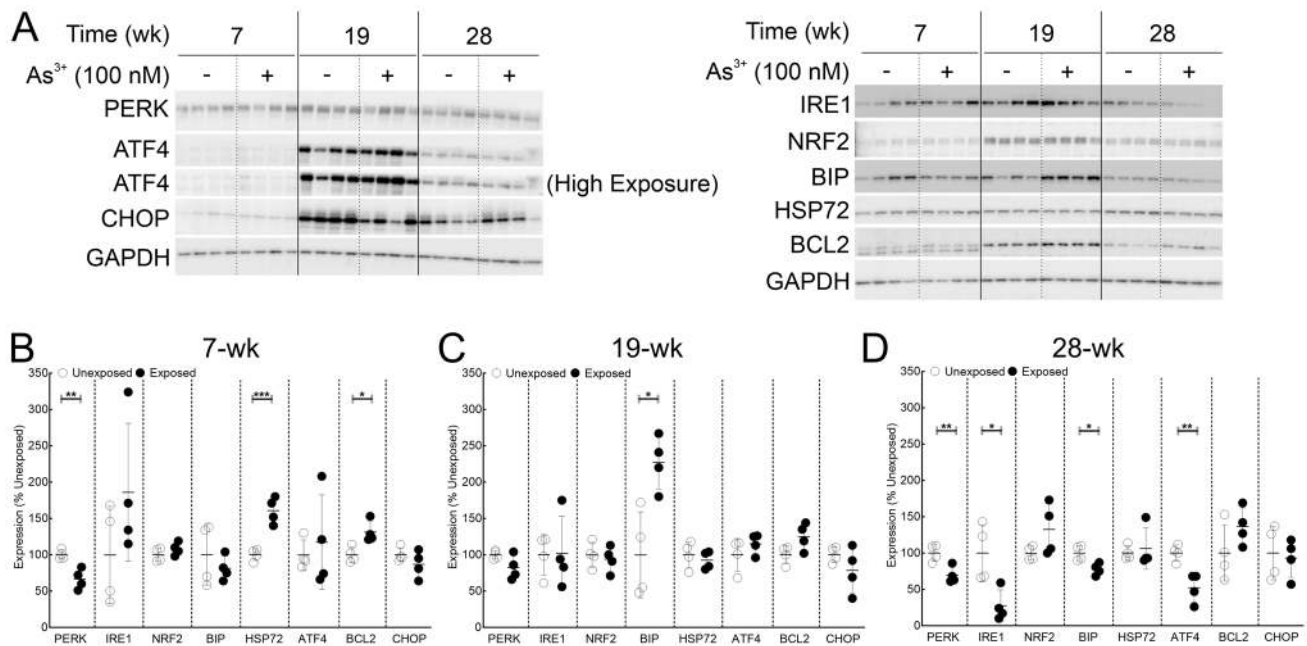


Fig. 4 Immunoblot analysis validates dysregulation of ER stress pathway predicted by RNA-seq data analyses at the protein level. **A** Immunoblot for ER stress markers at 7, 19 and 28-wk time points in HaCaT cells exposed to 100 nM As^{3+} or passage matched unexposed controls. **B** Densitometric analysis of ER stress marker expression at 7-wk. **C** Densitometric analysis of ER stress marker expression

at 19-wk. **D** Densitometric analysis of ER stress marker expression at 28-wk. Protein expression data in panels **B–D** are plotted as means \pm SD and expressed as % mean unexposed. Statistical analysis was done by unpaired two-tailed *t*-test; * $p \leq 0.05$, ** $p \leq 0.01$; *** $p \leq 0.001$

et al. 2018a; Bustaffa et al. 2014; Cardoso et al. 2018). However, a considerable knowledge gap exists in understanding the molecular processes that are operative in the interim between the beginning of exposure and the time cells are fully transformed.

The current study aims to fill this gap in the existing literature by providing a comprehensive picture of the molecular events at three stages of arsenic-induced carcinogenesis (early transformation related changes at 7-wk, transformation initiation at 19-wk and fully transformed at 28-wk). For this purpose, we combined longitudinal study design using passage-matched independent quadruplicate biological replicates along with large-scale genome-wide RNA-seq platform. This approach ensured that the analyses have considerable power to rule out random stochastic events as false positives or negatives while generating high-quality in-depth data. The passage matching was an important aspect in our study to rule out the effect of long passaging time. It is evident that several molecules follow a temporal variation in expression pattern irrespective of the exposure status (ATF4, BCL2, IRE1, NRF2 and CHOP in Fig. 4). While the reasons for this observation are not clear, it is certain that without appropriate passage matching, the robustness of our analyses would have been seriously compromised.

We unequivocally demonstrate temporally modulated changes in the growth patterns in the As^{3+} exposed HaCaT

cells (Fig. 1) in agreement with data from other groups (Pi et al. 2008; Sun et al. 2009). The slower growth rates in As^{3+} exposed cells at early stages of exposure could reflect the well-characterized cell cycle arrest/delay effects of As^{3+} exposure (Al-Eryani et al. 2017; States 2015; States et al. 2002; Tam et al. 2020). This inference is supported by the pathway analysis which shows a multitude of cell cycle related pathways being dysregulated at 7-wk (Fig. 3B, Supplementary Table 5 and Supplementary Fig. 2). In the next phase between 7 and 19-wk, there is a clear switch in the growth rate and a concomitant reversal of expression pattern of epithelial marker ZO-1 and mesenchymal marker Slug (Fig. 1B, D) which signals the initiation of EMT. Finally, at 28-wk, the growth rate of As^{3+} -exposed cells far exceeds that of passage matched unexposed controls, along with the reversal of the expression profiles of all the EMT markers tested (Fig. 1B, E), telltale signatures of carcinogenic transformation (Brabletz et al. 2018; Mehrara et al. 2007).

Our RNA-seq analyses show that multitudes of mRNAs and miRNAs targeting those mRNAs are differentially expressed in a time dependent manner (Fig. 2). Interestingly, the majority of the differentially expressed miRNA and mRNA molecules at each time point (corresponding to different stages in cancer development) are largely unique, as are the predicted activated/inhibited pathways they populate (Fig. 2 and Fig. 3). This limited longitudinal overlap between

the differentially expressed miRNAs or mRNAs suggest that the changing landscape of differentially expressed miRNAs might be contributing considerably to the changing landscape of differentially expressed mRNAs at each time point. Moreover, the mRNA expression alone may be a poor surrogate to understand exactly the impact of these changes in mRNA expression. Secondly, pathway analyses of differentially expressed mRNA targets of differentially expressed miRNAs at each time point show a great degree of overlap in the predicted canonical pathways with those of all differentially expressed mRNAs at those time points (Fig. 3E). Consequently, it is reasonable to hypothesize that the predicted alterations in the canonical pathways are largely guided by differential expression of mRNAs that are being targeted by the differentially expressed miRNAs at that time point. Thirdly, the fact that analysis of a subset of the differentially expressed mRNAs produces results similar to that of the entire dataset points to the robustness of the data and the analyses performed. Taken together, it is possible that at each stage, a new set of key molecules are being induced/suppressed that could be bringing about molecular changes associated with the sequential process of carcinogenesis.

Interestingly, only one pathway (osteoarthritis pathway) was found to be dysregulated at all three-time points (activated at 7-wk, inhibited at 19 and 28-wk) both in the differentially expressed mRNA (Fig. 3B) as well as differentially expressed mRNA targets of differentially expressed miRNA datasets (Supplementary Fig. 1). Furthermore, one more pathway (hepatic fibrosis signaling pathway) was found to be inhibited across all three-time points in the differentially expressed mRNA targets of differentially expressed miRNA datasets (Supplementary Fig. 1). While these pathways apparently have little to do with skin carcinogenesis, a closer look at the dysregulated molecules yield some interesting insights (Supplementary Fig. 3). Several of the dysregulated molecules, including molecules in the MAP kinase pathway, Rho signaling, TGF- β signaling, and MMPs, are involved in multiple cellular processes and are well-known players in the carcinogenesis of multiple organs (Derynck et al. 2021; Gialeli et al. 2011; Goel and Mercurio 2013; Huebner et al. 2019; Vella et al. 2018).

However, the question remains how these changes might usher in the changes that ultimately culminate in carcinogenesis. Pathway analysis data from this study shed some interesting light in this regard. Several of the top predicted canonical pathways at each time point reflect well-established mechanisms previously implicated in arsenic-induced carcinogenesis. At 7-wk, there is clear evidence of dysregulation of several cell cycle-related pathways (Supplementary Fig. 4). This observation is consistent with the widely accepted hypothesis that cell cycle dysregulation is an early event in arsenic-induced carcinogenesis (Al-Eryani et al. 2017; Hunt et al. 2014; States 2015; Tam et al. 2020; Zhou

and Xi 2018). Interestingly, the nucleotide excision repair (NER) pathway is induced at 7-wk (Fig. 3B and Supplementary Table 5). As³⁺ exposure is reported to inhibit the function of the NER pathway in human lung fibroblast cell line IMR-90 and mouse primary keratinocytes, albeit with much higher (10–40 μ M) acute (24 h) As³⁺ exposure (Holcomb et al. 2017). Furthermore, single nucleotide polymorphisms in several NER pathway genes have been demonstrated to be associated with arsenic-induced skin cancer development (Applebaum et al. 2007; Banerjee et al. 2007) and heightened chromosomal aberration in chronically exposed human populations (Banerjee et al. 2007). It is possible that the induction in the NER pathway (Supplementary Table 5) is a homeostatic response to alleviate the reduced function upon As³⁺ exposure. Notably, in our analysis, the z-score for the NER pathway drops sharply from 6.47 in the differentially expressed mRNA dataset (Supplementary Table 5) to 2.496 in the differentially expressed mRNA targets of differentially expressed miRNA (Supplementary Table 6). This suggests that many of the differentially expressed NER pathway molecules could be modulated by feedback between the protein and mRNA levels independent of miRNA regulation.

Analyses of differentially expressed mRNAs at 19-wk reveal dysregulation of a plethora of transformation-related pathways including Rho-GTPase signaling and nuclear hormone receptor pathways. Activation of Rho-GTPases is a central and critical event in carcinogenesis (Alan and Lundquist 2013; Aspenstrom 2018). It is therefore not surprising to find a significant inhibition of Rho-GTPase signaling pathway (Fig. 3B and Supplementary Table 5) in our dataset and probably represents a homeostatic mechanism to curb the effects of heightened signaling upon chronic As³⁺ exposure as the cells are undergoing transformation initiation. Furthermore, several nuclear hormone receptor signaling pathways are also predicted to be dysregulated, including androgen signaling, estrogen receptor signaling and prolactin signaling (Fig. 3B, Supplementary Table 5 and Supplementary Fig. 5). These pathways are known to be dysregulated in multiple cancer types including hormone independent melanoma and non-melanoma skin cancers and are often targets for chemotherapeutic intervention (Chan et al. 2018; Dika et al. 2019; Hua et al. 2018; Karayazi Atici et al. 2020; Mal et al. 2020; Pisano et al. 2021; Porter et al. 2019; Rajabi et al. 2017; Xiao et al. 2019). As³⁺ exposure at the environmentally relevant level of 100 nM for 48 h was found to suppress the expression of ER α mRNA and protein in MCF-7 cells and bind competitively to its hormone binding domain with K_i of 5 nM, modulating its downstream signaling (Davey et al. 2007; Stoica et al. 2000; Watson and Yager 2007). Furthermore, such low As³⁺ exposure (100–700 nM) using a hepatoma cell line has also been shown to inhibit transcription of androgen receptor signaling modulated target molecules, possibly by interaction with its zinc finger

containing DNA binding domain (Bodwell et al. 2006; Watson and Yager 2007). Dysregulation of these pathways are instrumental in EMT (Di Zazzo et al. 2019; Voutsadakis 2016; Yoriki et al. 2019), and perhaps unsurprisingly, we observe first signs of EMT in As³⁺ exposed cells at this time point. Our data thus clearly demonstrate hallmarks of transformation initiation in As³⁺ exposed HaCaT cells at 19-wk.

Data at 28-wk time point also reveal dysregulation of several critical pathways classically associated with a wide variety of cancers. e-NOS signaling, a master regulator of cancer development (Khan et al. 2020) including skin cancer (Bruch-Gerharz et al. 1998; Dhar et al. 2002), is inhibited (Fig. 3B and Supplementary Table 5). Such inhibition is well characterized to promote tumor growth (Xu et al. 2002). Dysregulated NOS signaling in turn leads to ER stress (Gotoh and Mori 2006) and subsequently modulates unfolded protein response (UPR) (Nakato et al. 2015). Both ER stress and UPR are predicted to be dysregulated at 28-wk time point (Fig. 3B, Supplementary Table 5 and Supplementary Fig. 6). ER stress initially brings about induction in the translation of ATF4 and modulation of macroautophagy and apoptosis but this ATF4 induction is abrogated under circumstances of prolonged ER stress (Rozpedek et al. 2016). In agreement, our data show a trend of induction for ATF4 at 7-wk (not significant) with significant suppression at 28-wk (Fig. 4). In addition, we also demonstrate that ER stress is invoked via the PERK arm at 7wk, whereas, at 28-wk, all three arms (PERK, IRE1 and ATF4) are involved. Our data thus reflect prolonged molecular stress that could play a key role in carcinogenesis upon chronic As³⁺ exposure. Dysregulation of ER stress pathway leads to UPR (Pallmann et al. 2019) and cancer (Wortel et al. 2017) both of which are occurring at the 28-wk time point in As³⁺-exposed cells. UPR is inhibited by proteasomal inhibition (Amanso et al. 2011; Lee et al. 2003) and dysregulated proteasome is itself a hallmark of cancer (Morozov and Karpov 2019). UPR thus is a key process bringing about molecular cross-talk between the two arms of protein degradation pathway, viz., ubiquitin-proteasome system and ER stress-induced autophagy. This cross-talk could mean that chronic As³⁺ exposure brings about proteome-wide changes not only by modulating the epigenome and the transcriptome, but also the cellular degradome, as recent studies suggest (Dodson et al. 2018; Tam and Wang 2020).

This interaction may also explain in part why we have some discordance in protein and RNA-seq data for a few of the EMT markers and ER stress molecules we tested (Figs. 1 and 4). Other explanations are also possible. For example, while tarbase predicts that *ERN1* (gene encoding IRE1) is targeted by miR-let7 (Karagkouni et al. 2018), which is induced in our 19 and 28-wk dataset (Supplementary Table 2), IPA does not show this in their miRNA-mRNA expression pairing (Supplementary Table 4). Thus,

the predictions of miRNA-mRNA pairing can be discordant in the databases. Additionally, several miRNAs lead to translation repression of the target proteins without altering the mRNA levels (Bhattacharyya et al. 2006; Wilczynska and Bushell 2015), such as those of ZO-1 (mir-34 at 7-wk; miR-let7 at 28-wk), β -Catenin (mir-200a at 28-wk), Slug (miR-218 at 28-wk) and N-Cadherin (mir-181b at 28-wk).

Additionally, this also partly explains why we see a considerable discordance in our miRNA-mRNA expression pairing. Our data demonstrate that several differentially expressed miRNA molecules are potentially able to modulate the expression of one differentially expressed target mRNA molecule (Supplementary Table 4). However, in the cellular context, it is likely that only one of the differentially expressed miRNAs is actually targeting the differentially expressed mRNA molecule rather than all the miRNAs together. For example, in our 7-wk dataset (Supplementary Table 4), AQP3 mRNA is induced and can be targeted by 4 distinct differentially expressed miRNAs (hsa-miR-222, hsa-miR-3661, hsa-miR-663b; all induced and hsa-miR-4688; suppressed). It is possible that in the cells, only the hsa-miR-4688 is actually regulating the expression of AQP3 mRNA, although, all the other three are also potentially capable of doing so. Another possibility is that AQP3 is induced at the mRNA level and the induction of one or more targeting miRNAs (hsa-miR-222, hsa-miR-3661, hsa-miR-663b) is actually a homeostatic response to bring down the expression of AQP3 mRNA to the basal level. Together, these observations suggest that while expression pairing is an important and useful tool to categorize possible miRNA-mRNA interactions in a large dataset, further experimental validation needs to be performed to elucidate the nature of these predicted pairings, both at the mRNA and protein level.

The present work provides a much-needed picture of the sequence of molecular events taking place at each phase of carcinogenic transformation by chronic As³⁺ exposure in a well-established model of arsenic-induced cSCC. The events change dynamically with time and consist of several alterations that are consistent both with As³⁺ exposure as well as established mechanisms of carcinogenesis in the skin and other organs. In addition, we also provide considerable validation of transcriptomic prediction at the protein level in multiple molecules spanning three different branches of the ER stress pathway. This work thus presents a framework for understanding the events leading from exposure initiation through to transformation. Together, our data provide strong evidence as to how different molecules and pathways known to be dysregulated individually in cancer and upon As³⁺ exposure interact as complex coordinated networks (Supplementary Fig. 4–6) to bring about cellular changes at successive steps in the process of As³⁺-induced skin carcinogenesis at toxicologically relevant exposure conditions.

This work and the existing dataset open up possibilities of future studies to empirically address the effects of stochasticity in carcinogenesis as well as the efficacy of passage matching for chronic exposure scenarios. Finally, it would be imperative to study proteome-wide changes brought about by chronic As³⁺ exposure in a similar model to understand how the proteomic and transcriptomic changes are correlated in the process of carcinogenesis.

Supplementary Information The online version contains supplementary material available at <https://doi.org/10.1007/s00204-021-03084-2>.

Acknowledgements The authors thank Ms. Elizabeth Ann Hudson, Research Associate, Center for Genetics and Molecular Medicine, University of Louisville, Louisville, KY, USA, for her technical expertise with RNA-seq experiments. The authors also thank Dr. Walter H. Watson, Associate Professor, Departments of Pharmacology & Toxicology and Medicine, University of Louisville, Louisville, KY, USA, for his helpful critique and suggestions during the preparation of this manuscript.

Author contributions MB: conceived or designed the study, performed the research, analyzed the data and wrote the paper. APFC and LAE: performed the research, analyzed the data. JP, TSK, SS, and SNR: contributed new methods or models and analyzed the data. JCS: conceived or designed the study and wrote the paper. All the authors participated in reviewing and editing the paper.

Funding This study was supported by National Institute of Environmental Health Sciences grants R21ES023627 (JCS), R21ES030334 (JCS), R01ES027778 (JCS) and P30ES030283 (JCS).

Data availability All the transcriptomic data have been deposited to appropriate databases (accession numbers are provided in the materials and methods sections). All other data/material generated as a part of this work are available upon request.

Code availability Not applicable.

Declarations

Conflict of interest The authors declare no actual or potential conflict of interest/competing financial interest.

Ethics approval Not applicable.

Consent to participate Not applicable.

Consent for publication All the co-authors have read and agreed to submit the manuscript for publication in its present form.

Open Access This article is licensed under a Creative Commons Attribution 4.0 International License, which permits use, sharing, adaptation, distribution and reproduction in any medium or format, as long as you give appropriate credit to the original author(s) and the source, provide a link to the Creative Commons licence, and indicate if changes were made. The images or other third party material in this article are included in the article's Creative Commons licence, unless indicated otherwise in a credit line to the material. If material is not included in the article's Creative Commons licence and your intended use is not permitted by statutory regulation or exceeds the permitted use, you will

need to obtain permission directly from the copyright holder. To view a copy of this licence, visit <http://creativecommons.org/licenses/by/4.0/>.

References

- Alan JK, Lundquist EA (2013) Mutationally activated Rho GTPases in cancer. *Small GTPases* 4(3):159–163. <https://doi.org/10.4161/sgtp.26530>
- Al-Eryani L (2017) MiRNA expression changes in arsenic-induced skin cancer in vitro and in vivo. Ph.D. Dissertation, University of Louisville
- Al-Eryani L, Waigel S, Jala V, Jenkins SF, Christopher States J (2017) Cell cycle pathway dysregulation in human keratinocytes during chronic exposure to low arsenite. *Toxicol Appl Pharmacol*. 331:130–134. <https://doi.org/10.1016/j.taap.2017.06.002>
- Al-Eryani L, Jenkins SF, States VA et al (2018a) miRNA expression profiles of premalignant and malignant arsenic-induced skin lesions. *PLoS ONE* 13(8):e0202579. <https://doi.org/10.1371/journal.pone.0202579>
- Al-Eryani L, Waigel S, Tyagi A et al (2018b) Differentially expressed mRNA targets of differentially expressed miRNAs predict changes in the TP53 axis and carcinogenesis-related pathways in human keratinocytes chronically exposed to arsenic. *Toxicol Sci* 162(2):645–654. <https://doi.org/10.1093/toxsci/kfx292>
- Amanso AM, Debbas V, Laurindo FR (2011) Proteasome inhibition represses unfolded protein response and Nox4, sensitizing vascular cells to endoplasmic reticulum stress-induced death. *PLoS ONE* 6(1):e14591. <https://doi.org/10.1371/journal.pone.0014591>
- Applebaum KM, Karagas MR, Hunter DJ et al (2007) Polymorphisms in nucleotide excision repair genes, arsenic exposure, and non-melanoma skin cancer in New Hampshire. *Environ Health Perspect* 115(8):1231–1236. <https://doi.org/10.1289/ehp.10096>
- Aspenstrom P (2018) Activated Rho GTPases in Cancer-The Beginning of a New Paradigm. *Int J Mol Sci* 19(12):3949. <https://doi.org/10.3390/ijms19123949>
- Banerjee M, Sarkar J, Das JK et al (2007) Polymorphism in the ERCC2 codon 751 is associated with arsenic-induced premalignant hyperkeratosis and significant chromosome aberrations. *Carcinogenesis* 28(3):672–676. <https://doi.org/10.1093/carcin/bgl181>
- Banerjee M, Bhattacharjee P, Giri AK (2011) Arsenic-induced cancers: a review with special reference to gene, environment and their interaction. *Genes and Environment* 33(4):128–140
- Banerjee M, Ferragut Cardoso AP, Lykoudi A et al (2020) Arsenite exposure displaces zinc from ZRANB2 leading to altered splicing. *Chem Res Toxicol*. 33(6):1403–1417
- Bhattacharyya SN, Habermacher R, Martine U, Closs EI, Filipowicz W (2006) Relief of microRNA-mediated translational repression in human cells subjected to stress. *Cell* 125(6):1111–1124. <https://doi.org/10.1016/j.cell.2006.04.031>
- Bodwell JE, Gosse JA, Nomikos AP, Hamilton JW (2006) Arsenic disruption of steroid receptor gene activation: complex dose-response effects are shared by several steroid receptors. *Chem Res Toxicol* 19(12):1619–1629. <https://doi.org/10.1021/tx060122q>
- Bolger AM, Lohse M, Usadel B (2014) Trimmomatic: a flexible trimmer for Illumina sequence data. *Bioinformatics* 30(15):2114–2120. <https://doi.org/10.1093/bioinformatics/btu170>
- Boukamp P, Petrussevska RT, Breitkreutz D, Hornung J, Markham A, Fusenig NE (1988) Normal keratinization in a spontaneously immortalized aneuploid human keratinocyte cell line. *J Cell Biol* 106(3):761–771. <https://doi.org/10.1083/jcb.106.3.761>
- Brabletz T, Kalluri R, Nieto MA, Weinberg RA (2018) EMT in cancer. *Nat Rev Cancer* 18(2):128–134. <https://doi.org/10.1038/nrc.2017.118>

- Bruch-Gerharz D, Ruzicka T, Kolb-Bachofen V (1998) Nitric oxide and its implications in skin homeostasis and disease - a review. *Arch Dermatol Res* 290(12):643–651. <https://doi.org/10.1007/s004030050367>
- Bustaffa E, Stoccoro A, Bianchi F, Migliore L (2014) Genotoxic and epigenetic mechanisms in arsenic carcinogenicity. *Arch Toxicol* 88(5):1043–1067. <https://doi.org/10.1007/s00204-014-1233-7>
- Calabrese EJ, Baldwin LA (2003) Inorganics and hormesis. *Crit Rev Toxicol* 33(3–4):215–304. <https://doi.org/10.1080/713611040>
- Cardoso APF, Al-Eryani L, States JC (2018) Arsenic-induced carcinogenesis: the impact of miRNA dysregulation. *Toxicol Sci* 165(2):284–290. <https://doi.org/10.1093/toxsci/kfy128>
- Chan JSK, Sng MK, Teo ZQ, Chong HC, Twang JS, Tan NS (2018) Targeting nuclear receptors in cancer-associated fibroblasts as concurrent therapy to inhibit development of chemoresistant tumors. *Oncogene* 37(2):160–173. <https://doi.org/10.1038/ncr.2017.319>
- Chen QY, Costa M (2018) PI3K/Akt/mTOR signaling pathway and the biphasic effect of arsenic in carcinogenesis. *Mol Pharmacol* 94(1):784–792. <https://doi.org/10.1124/mol.118.112268>
- Chen X, Cubillos-Ruiz JR (2020) Endoplasmic reticulum stress signals in the tumour and its microenvironment. *Nat Rev Cancer* 21:71–88. <https://doi.org/10.1038/s41568-020-00312-2>
- Cohen SM, Chowdhury A, Arnold LL (2016) Inorganic arsenic: a non-genotoxic carcinogen. *J Environ Sci (china)* 49:28–37. <https://doi.org/10.1016/j.jes.2016.04.015>
- Davey JC, Bodwell JE, Gosse JA, Hamilton JW (2007) Arsenic as an endocrine disruptor: effects of arsenic on estrogen receptor-mediated gene expression in vivo and in cell culture. *Toxicol Sci* 98(1):75–86. <https://doi.org/10.1093/toxsci/kfm013>
- Derynck R, Turley SJ, Akhurst RJ (2021) TGFbeta biology in cancer progression and immunotherapy. *Nat Rev Clin Oncol* 18(1):9–34. <https://doi.org/10.1038/s41571-020-0403-1>
- Dhar A, Young MR, Colburn NH (2002) The role of AP-1, NF-kappaB and ROS/NOS in skin carcinogenesis: the JB6 model is predictive. *Mol Cell Biochem* 234–235(1–2):185–193
- Di Zazzo E, Galasso G, Giovannelli P et al (2019) Estrogen receptors in epithelial-mesenchymal transition of prostate cancer. *Cancers (Basel)* 11(10):1418. <https://doi.org/10.3390/cancers11101418>
- Dika E, Patrizi A, Lambertini M et al (2019) Estrogen Receptors and Melanoma: a review. *Cells* 8(11):1463
- Dobin A, Gingeras TR (2015) Mapping RNA-seq reads with STAR. *Curr Protoc Bioinformatics* 51:11.14.1–11.14.19. <https://doi.org/10.1002/0471250953.bi1114s1>
- Dobin A, Davis CA, Schlesinger F et al (2013) STAR: ultrafast universal RNA-seq aligner. *Bioinformatics* 29(1):15–21. <https://doi.org/10.1093/bioinformatics/bts635>
- Dodson M, de la Vega MR, Harder B et al (2018) Low-level arsenic causes proteotoxic stress and not oxidative stress. *Toxicol Appl Pharmacol* 341:106–113. <https://doi.org/10.1016/j.taap.2018.01.014>
- Friedlander MR, Mackowiak SD, Li N, Chen W, Rajewsky N (2012) miRDeep2 accurately identifies known and hundreds of novel microRNA genes in seven animal clades. *Nucleic Acids Res* 40(1):37–52. <https://doi.org/10.1093/nar/gkr688>
- Ghosh P, Banerjee M, De Chaudhuri S et al (2007) Comparison of health effects between individuals with and without skin lesions in the population exposed to arsenic through drinking water in West Bengal. *India J Expo Sci Environ Epidemiol* 17(3):215–223. <https://doi.org/10.1038/sj.jes.7500510>
- Gialeli C, Theocharis AD, Karamanos NK (2011) Roles of matrix metalloproteinases in cancer progression and their pharmacological targeting. *FEBS J* 278(1):16–27. <https://doi.org/10.1111/j.1742-4658.2010.07919.x>
- Goel HL, Mercurio AM (2013) VEGF targets the tumour cell. *Nat Rev Cancer* 13(12):871–882. <https://doi.org/10.1038/nrc3627>
- Gonsebatt ME, Vega L, Montero R et al (1994) Lymphocyte replicating ability in individuals exposed to arsenic via drinking water. *Mutat Res* 313(2–3):293–299. [https://doi.org/10.1016/0165-1161\(94\)90059-0](https://doi.org/10.1016/0165-1161(94)90059-0)
- Gonsebatt ME, Vega L, Salazar AM et al (1997) Cytogenetic effects in human exposure to arsenic. *Mutat Res* 386(3):219–228. [https://doi.org/10.1016/s1383-5742\(97\)00009-4](https://doi.org/10.1016/s1383-5742(97)00009-4)
- Gotoh T, Mori M (2006) Nitric oxide and endoplasmic reticulum stress. *Arterioscler Thromb Vasc Biol* 26(7):1439–1446. <https://doi.org/10.1161/01.ATV.0000223900.67024.15>
- Guo Z, Hu Q, Tian J et al (2016) Proteomic profiling reveals candidate markers for arsenic-induced skin keratosis. *Environ Pollut* 218:34–38. <https://doi.org/10.1016/j.envpol.2016.08.035>
- Hashmi MZ, Naveedullah SH, Zhu S, Yu C, Shen C (2014) Growth, bioluminescence and shoal behavior hormetic responses to inorganic and/or organic chemicals: a review. *Environ Int* 64:28–39. <https://doi.org/10.1016/j.envint.2013.11.018>
- Holcomb N, Goswami M, Han SG et al (2017) Inorganic arsenic inhibits the nucleotide excision repair pathway and reduces the expression of XPC. *DNA Repair (amst)* 52:70–80. <https://doi.org/10.1016/j.dnarep.2017.02.009>
- Hua H, Zhang H, Kong Q, Jiang Y (2018) Mechanisms for estrogen receptor expression in human cancer. *Exp Hematol Oncol* 7:24. <https://doi.org/10.1186/s40164-018-0116-7>
- Huang HW, Lee CH, Yu HS (2019) Arsenic-Induced Carcinogenesis and Immune Dysregulation. *Int J Environ Res Public Health* 16(15):2746. <https://doi.org/10.3390/ijerph16152746>
- Huebner K, Prochazka J, Monteiro AC, Mahadevan V, Schneider-Stock R (2019) The activating transcription factor 2: an influencer of cancer progression. *Mutagenesis* 34(5–6):375–389. <https://doi.org/10.1093/mutage/gez041>
- Hunt KM, Srivastava RK, Elmets CA, Athar M (2014) The mechanistic basis of arsenicosis: pathogenesis of skin cancer. *Cancer Lett* 354(2):211–219. <https://doi.org/10.1016/j.canlet.2014.08.016>
- IARC (2012) Special report: policy, a review of human carcinogens—part c: metals, arsenic, dusts, and fibres. *IARC Monogr Eval Carcinog Risks Hum* 100:11–465
- Karagas MR, Gossai A, Pierce B, Ahsan H (2015) Drinking water arsenic contamination, skin lesions, and malignancies: a systematic review of the global evidence. *Curr Environ Health Rep* 2(1):52–68. <https://doi.org/10.1007/s40572-014-0040-x>
- Karagkouni D, Paraskevopoulou MD, Chatzopoulos S et al (2018) DIANA-TarBase v8: a decade-long collection of experimentally supported miRNA-gene interactions. *Nucleic Acids Res* 46(D1):D239–D245. <https://doi.org/10.1093/nar/gkx1141>
- Karayazi Atici O, Govindarajan N, Lopetegui-Gonzalez I, Shemanko CS (2020) Prolactin: a hormone with diverse functions from mammary gland development to cancer metastasis. *Semin Cell Dev Biol* 114:159–170. <https://doi.org/10.1016/j.semedb.2020.10.005>
- Khan FH, Dervan E, Bhattacharyya DD, McAuliffe JD, Miranda KM, Glynn SA (2020) The Role of Nitric Oxide in Cancer: Master Regulator or NOT? *Int J Mol Sci* 21(24):9393. <https://doi.org/10.3390/ijms21249393>
- Lee CH, Yu HS (2016) Role of mitochondria, ROS, and DNA damage in arsenic induced carcinogenesis. *Front Biosci (schol Ed)* 8:312–320. <https://doi.org/10.2741/s465>
- Lee AH, Iwakoshi NN, Anderson KC, Glimcher LH (2003) Proteasome inhibitors disrupt the unfolded protein response in myeloma cells. *Proc Natl Acad Sci USA* 100(17):9946–9951. <https://doi.org/10.1073/pnas.1334037100>
- Liao Y, Smyth GK, Shi W (2013) The Subread aligner: fast, accurate and scalable read mapping by seed-and-vote. *Nucleic Acids Res* 41(10):e108. <https://doi.org/10.1093/nar/gkt214>
- Mal R, Magner A, David J et al (2020) Estrogen receptor beta (ERbeta): a ligand activated tumor suppressor. *Front Oncol* 10:587386. <https://doi.org/10.3389/fonc.2020.587386>

- Martin M (2011) Cutadapt removes adapter sequences from high-throughput sequencing reads. *EMBnet J* 17(1):10–12. <https://doi.org/10.14806/ej.17.1.200>.
- McCarthy DJ, Chen Y, Smyth GK (2012) Differential expression analysis of multifactor RNA-Seq experiments with respect to biological variation. *Nucleic Acids Res* 40(10):4288–4297. <https://doi.org/10.1093/nar/gks042>
- Mehrara E, Forssell-Aronsson E, Ahlman H, Bernhardt P (2007) Specific growth rate versus doubling time for quantitative characterization of tumor growth rate. *Cancer Res* 67(8):3970–3975. <https://doi.org/10.1158/0008-5472.CAN-06-3822>
- Mir SA, Pinto SM, Paul S et al (2017) SILAC-based quantitative proteomic analysis reveals widespread molecular alterations in human skin keratinocytes upon chronic arsenic exposure. *Proteomics* 17(6). <https://doi.org/10.1002/ptm.201600257>
- Morozov AV, Karpov VL (2019) Proteasomes and several aspects of their heterogeneity relevant to cancer. *Front Oncol* 9:761. <https://doi.org/10.3389/fonc.2019.00761>
- Nakato R, Ohkubo Y, Konishi A et al (2015) Regulation of the unfolded protein response via S-nitrosylation of sensors of endoplasmic reticulum stress. *Sci Rep* 5:14812. <https://doi.org/10.1038/srep14812>
- Naujokas MF, Anderson B, Ahsan H et al (2013) The broad scope of health effects from chronic arsenic exposure: update on a worldwide public health problem. *Environ Health Perspect* 121(3):295–302. <https://doi.org/10.1289/ehp.1205875>
- Nigra AE, Chen Q, Chillrud SN et al (2020) Inequalities in public water arsenic concentrations in counties and community water systems across the United States, 2006–2011. *Environ Health Perspect* 128(12):127001. <https://doi.org/10.1289/EHP7313>
- Pallmann N, Livgard M, Tesikova M et al (2019) Regulation of the unfolded protein response through ATF4 and FAM129A in prostate cancer. *Oncogene* 38(35):6301–6318. <https://doi.org/10.1038/s41388-019-0879-2>
- Pi J, Kumagai Y, Sun G et al (2000) Decreased serum concentrations of nitric oxide metabolites among Chinese in an endemic area of chronic arsenic poisoning in inner Mongolia. *Free Radic Biol Med* 28(7):1137–1142. [https://doi.org/10.1016/s0891-5849\(00\)00209-4](https://doi.org/10.1016/s0891-5849(00)00209-4)
- Pi J, Diwan BA, Sun Y et al (2008) Arsenic-induced malignant transformation of human keratinocytes: involvement of Nrf2. *Free Radic Biol Med* 45(5):651–658. <https://doi.org/10.1016/j.freeradbiomed.2008.05.020>
- Pisano C, Tucci M, Di Stefano RF et al (2021) Interactions between androgen receptor signaling and other molecular pathways in prostate cancer progression: Current and future clinical implications. *Crit Rev Oncol Hematol* 157:103185. <https://doi.org/10.1016/j.critrevonc.2020.103185>
- Podgorski J, Berg M (2020) Global threat of arsenic in groundwater. *Science* 368(6493):845–850. <https://doi.org/10.1126/science.aba1510>
- Porter BA, Ortiz MA, Bratslavsky G, Kotula L (2019) Structure and Function of the Nuclear Receptor Superfamily and Current Targeted Therapies of Prostate Cancer. *Cancers (Basel)* 11(12):1852. <https://doi.org/10.3390/cancers11121852>
- Rajabi P, Bagheri M, Hani M (2017) Expression of estrogen receptor alpha in malignant melanoma. *Adv Biomed Res* 6:14. <https://doi.org/10.4103/2277-9175.200789>
- R-Core-Team (2018) R: A language and environment for statistical computing. R Foundation for Statistical Computing, Vienna, Austria
- Robinson MD, Oshlack A (2010) A scaling normalization method for differential expression analysis of RNA-seq data. *Genome Biol* 11(3):R25. <https://doi.org/10.1186/gb-2010-11-3-r25>
- Robinson MD, Smyth GK (2008) Small-sample estimation of negative binomial dispersion, with applications to SAGE data. *Biostatistics* 9(2):321–332. <https://doi.org/10.1093/biostatistics/kxm030>
- Robinson MD, McCarthy DJ, Smyth GK (2010) edgeR: a bioconductor package for differential expression analysis of digital gene expression data. *Bioinformatics* 26(1):139–140. <https://doi.org/10.1093/bioinformatics/btp616>
- Rozpedek W, Pytel D, Mucha B, Leszczynska H, Diehl JA, Majsterek I (2016) The role of the PERK/eIF2alpha/ATF4/CHOP signaling pathway in tumor progression during endoplasmic reticulum stress. *Curr Mol Med* 16(6):533–544. <https://doi.org/10.2174/1566524016666160523143937>
- Schneider CA, Rasband WS, Eliceiri KW (2012) NIH Image to ImageJ: 25 years of image analysis. *Nat Methods* 9(7):671–675
- Schneider VA, Graves-Lindsay T, Howe K et al (2017) Evaluation of GRCh38 and de novo haploid genome assemblies demonstrates the enduring quality of the reference assembly. *Genome Res* 27(5):849–864. <https://doi.org/10.1101/gr.213611.116>
- States JC (2015) Disruption of mitotic progression by arsenic. *Biol Trace Elem Res* 166(1):34–40. <https://doi.org/10.1007/s12011-015-0306-7>
- States JC, Reiners JJ Jr, Pounds JG et al (2002) Arsenite disrupts mitosis and induces apoptosis in SV40-transformed human skin fibroblasts. *Toxicol Appl Pharmacol* 180(2):83–91. <https://doi.org/10.1006/taap.2002.9376>
- Stoica A, Pentecost E, Martin MB (2000) Effects of arsenite on estrogen receptor-alpha expression and activity in MCF-7 breast cancer cells. *Endocrinology* 141(10):3595–3602. <https://doi.org/10.1210/endo.141.10.7704>
- Sun Y, Pi J, Wang X, Tokar EJ, Liu J, Waalkes MP (2009) Aberrant cyokeratin expression during arsenic-induced acquired malignant phenotype in human HaCaT keratinocytes consistent with epidermal carcinogenesis. *Toxicology* 262(2):162–170. <https://doi.org/10.1016/j.tox.2009.06.003>
- Surdu S (2014) Non-melanoma skin cancer: occupational risk from UV light and arsenic exposure. *Rev Environ Health* 29(3):255–264. <https://doi.org/10.1515/reveh-2014-0040>
- Tam LM, Wang Y (2020) Arsenic exposure and compromised protein quality control. *Chem Res Toxicol* 33(7):1594–1604. <https://doi.org/10.1021/acs.chemrestox.0c00107>
- Tam LM, Price NE, Wang Y (2020) Molecular mechanisms of arsenic-induced disruption of DNA repair. *Chem Res Toxicol* 33(3):709–726. <https://doi.org/10.1021/acs.chemrestox.9b00464>
- Tokar EJ XY, Waalkes MP (2016) Cancer Induced by Exposure to Arsenicals in Animals. In: States JC (ed) *Arsenic: Exposure Sources, Health Risks, and Mechanisms of Toxicity*. John Wiley & Sons, Inc., p 441–452
- Trapnell C, Roberts A, Goff L et al (2012) Differential gene and transcript expression analysis of RNA-seq experiments with TopHat and Cufflinks. *Nat Protoc* 7(3):562–578. <https://doi.org/10.1038/nprot.2012.016>
- Tukey JW (1949) Comparing individual means in the analysis of variance. *Biometrics* 5(2):99–114
- Vella V, Milluzzo A, Scalisi NM, Vigneri P, Sciacca L (2018) Insulin Receptor Isoforms in Cancer. *Int J Mol Sci* 19(11):3615. <https://doi.org/10.3390/ijms19113615>
- Voutsadakis IA (2016) Epithelial-mesenchymal transition (EMT) and regulation of emt factors by steroid nuclear receptors in breast cancer: a review and in silico investigation. *J Clin Med* 5(1):11. <https://doi.org/10.3390/jcm5010011>
- Waldman A, Schmults C (2019) Cutaneous squamous cell carcinoma. *Hematol Oncol Clin North Am* 33(1):1–12. <https://doi.org/10.1016/j.hoc.2018.08.001>
- Watson WH, Yager JD (2007) Arsenic: extension of its endocrine disruption potential to interference with estrogen receptor-mediated

- signaling. *Toxicol Sci* 98(1):1–4. <https://doi.org/10.1093/toxsci/kfm111>
- Wilczynska A, Bushell M (2015) The complexity of miRNA-mediated repression. *Cell Death Differ* 22(1):22–33. <https://doi.org/10.1038/cdd.2014.112>
- Wingett SW, Andrews S (2018) FastQ Screen: a tool for multi-genome mapping and quality control. *F1000Res* 7:1338. <https://doi.org/10.12688/f1000research.15931.2>
- Wortel IMN, van der Meer LT, Kilberg MS, van Leeuwen FN (2017) Surviving STRESS: MODULATION of ATF4-mediated stress responses in normal and malignant cells. *Trends Endocrinol Metab* 28(11):794–806. <https://doi.org/10.1016/j.tem.2017.07.003>
- Xiao L, Luo Y, Tai R, Zhang N (2019) Estrogen receptor beta suppresses inflammation and the progression of prostate cancer. *Mol Med Rep* 19(5):3555–3563. <https://doi.org/10.3892/mmr.2019.10014>
- Xu W, Liu LZ, Loizidou M, Ahmed M, Charles IG (2002) The role of nitric oxide in cancer. *Cell Res* 12(5–6):311–320. <https://doi.org/10.1038/sj.cr.7290133>
- Yoriki K, Mori T, Kokabu T et al (2019) Estrogen-related receptor alpha induces epithelial-mesenchymal transition through cancer-stromal interactions in endometrial cancer. *Sci Rep* 9(1):6697. <https://doi.org/10.1038/s41598-019-43261-z>
- Zerbino DR, Achuthan P, Akanni W et al (2018) Ensembl 2018. *Nucleic Acids Res* 46(D1):D754–D761. <https://doi.org/10.1093/nar/gkx1098>
- Zhou Q, Xi S (2018) A review on arsenic carcinogenesis: epidemiology, metabolism, genotoxicity and epigenetic changes. *Regul Toxicol Pharmacol* 99:78–88. <https://doi.org/10.1016/j.yrtph.2018.09.010>

Publisher's Note Springer Nature remains neutral with regard to jurisdictional claims in published maps and institutional affiliations.